

This work was written as part of one of the author's official duties as an Employee of the United States Government and is therefore a work of the United States Government. In accordance with 17 U.S.C. 105, no copyright protection is available for such works under U.S. Law. Access to this work was provided by the University of Maryland, Baltimore County (UMBC) ScholarWorks@UMBC digital repository on the Maryland Shared Open Access (MD-SOAR) platform.

Please provide feedback

Please support the ScholarWorks@UMBC repository by emailing scholarworks-group@umbc.edu and telling us what having access to this work means to you and why it's important to you. Thank you.

JGR Space Physics

RESEARCH ARTICLE

10.1029/2020JA027879

Key Points:

- Particle distribution functions in a reconnection diffusion region are reconstructed using a maximum entropy closure
- Kinetic features such as electron anisotropy and acceleration are reproduced
- Inclusion of fourth-order velocity moments allows the modeling of counterstreaming populations

Correspondence to:

J. Ng,
jonng@umd.edu

Citation:

Ng, J., Chen, L.-J., Hakim, A., & Bhattacharjee, A. (2020). Reconstruction of electron and ion distribution functions in a magnetotail reconnection diffusion region. *Journal of Geophysical Research: Space Physics*, 125, e2020JA027879. <https://doi.org/10.1029/2020JA027879>

Received 4 FEB 2020

Accepted 20 MAY 2020

Accepted article online 23 MAY 2020

Reconstruction of Electron and Ion Distribution Functions in a Magnetotail Reconnection Diffusion Region

Jonathan Ng^{1,2} , Li-Jen Chen³, Ammar Hakim⁴, and Amitava Bhattacharjee^{1,4,5}

¹Department of Astrophysical Sciences, Princeton University, Princeton, NJ, USA, ²Department of Astronomy, University of Maryland, College Park, MD, USA, ³NASA Goddard Space Flight Center, Greenbelt, MD, USA, ⁴Princeton Plasma Physics Laboratory, Princeton, NJ, USA, ⁵Princeton Center for Heliophysics, Princeton University, Princeton, NJ, USA

Abstract In the diffusion region of magnetotail reconnection, particle distributions are highly structured, exhibiting triangular shapes and multiple striations that deviate dramatically from the Maxwellian distribution. Fully kinetic simulations have been demonstrated to be capable of producing the essential structures of the observed distribution functions, yet are computationally not feasible for 3D global simulations. The fluid models used for large-scale simulations, on the other hand, do not have the kinetic physics necessary for describing reconnection accurately. Our study aims to bridge fully kinetic and fluid simulations by quantifying the information required to capture the non-Maxwellian features in the distributions underlying the closures used in the fluid code. We compare the results of fully kinetic simulations with observed electron velocity distributions in a magnetotail reconnection diffusion region and use the maximum entropy model to reconstruct electron and ion distributions using various numbers of moments obtained from the simulation. Our results indicate that using only local moments, the maximum entropy model can reproduce many of the features of the distributions: (1) the electron outflow distribution with a tilted triangular structure is reproduced with 21 or more moments in agreement with Ng et al. (2018, <https://doi.org/10.1063/1.5041758>) and (2) counterstreaming distributions can be captured with the 35-moment model when the separation in velocity space between the populations is large.

Plain Language Summary Fluid modeling of plasmas in collisionless environments such as the magnetosphere is challenging because the approximation that collisions are important does not hold. It is important to understand the motion of individual particles as collisions do not bring them back to equilibrium. However, this is computationally intensive and cannot be used to model the Earth at the present time. We use a recent fluid model which is based on maximizing the entropy of an underlying distribution of particles and attempt to reconstruct particle distributions during reconnection in the Earth's magnetotail. We show that most features of the distribution function can be reproduced using an increasing number of fluid moments.

1. Introduction

Non-Maxwellian particle velocity distributions prevail in weakly collisional plasma environments such as the magnetosphere. In particular, for magnetic reconnection regions in the magnetotail, strongly anisotropic electron velocity distributions with $p_{\parallel} > p_{\perp}$ are found in inflow regions (Øieroset et al., 2002), while triangular distributions with accelerated electrons are found within the electron diffusion region and close to the x-point during antiparallel reconnection (Torbert et al., 2018). The formation of these distributions can be explained by electron trapping in the inflow (Egedal et al., 2013), while in the electron diffusion region, the meandering electron orbits in the magnetic field reversal explains the striated and counterstreaming populations (Bessho et al., 2014, 2018; Fujimoto & Sydora, 2009; Ng et al., 2011, 2012).

Although kinetic physics is necessary to capture these structures which are dependent on the electron trajectories, fully kinetic simulations are computationally expensive, and many global simulations of magnetospheres use fluid models such as magnetohydrodynamics (MHD). There have been different approaches to incorporate physics beyond MHD in global simulations. This includes hybrid particle-in-cell (PIC) (Karimabadi et al., 2006; Lu et al., 2015) and Vlasov codes (Kempf et al., 2013; Palmroth et al., 2018), which simulate kinetic ions and fluid electrons. Another approach involves embedding PIC boxes within a

larger-scale MHD or two-fluid simulation, so that only the regions in which kinetic effects are thought to be important use a fully kinetic model (Fujimoto, 2018; Ho et al., 2018; Lautenbach & Grauer, 2018; Tóth et al., 2016, 2017).

The approach discussed in this paper involves extended fluid models which evolve the higher moments of the Vlasov equation (Hesse et al., 1995; Ng et al., 2017; Wang et al., 2015; Yin et al., 2001). In addition to the usual density and momentum moments, these models evolve the pressure tensor, which is important for balancing the reconnection electric field at the x-point. Observational validation tests of such models have produced encouraging results (Dong et al., 2019; Wang et al., 2018). However, closures for general plasma parameters are challenging to develop and these models do not capture all the kinetic physics, which can affect the reconnection rate and development of instabilities (Ng et al., 2017, 2019).

In this paper, we focus on what distribution function information can be obtained given a fixed number of known moments of velocity distribution functions. We use the maximum entropy closure (Levermore, 1996), which has the useful property that the derived fluid equations are hyperbolic. Our earlier work on using this closure to reconstruct electron distributions in reconnection regions has shown that the characteristic triangular shape can be recovered using 21 moments (the heat flux tensor and scalar v^4 moment) (Ng et al., 2018). In this study, we use parameters that are more relevant to the event reported by Torbert et al. (2018), and the distributions in the simulation are chosen to correspond to the observations. We also increase the number of moments kept to 35, thereby demonstrating the ability of the model to recover counterstreaming populations.

The remainder of this paper is organized as follows: in section 2, we review the derivation of the maximum closure and the fluid equations obtained, compared with the Chapman-Enskog and Grad approaches. In section 3, we perform comparisons between the electron distribution functions obtained from Magnetospheric Multiscale (MMS) observations, a kinetic simulation and reconstructions using successively higher numbers of moments. We then discuss the results in section 4 and the implications for fluid modeling.

2. Maximum Entropy Closure

Maximum entropy methods are used to determine probability distributions given limited information (Jaynes, 1957) and have been used in many scientific fields including astrophysics (Richstone & Tremaine, 1988), biology (Yeo & Burge, 2004), and natural language processing (Charniak, 2000). In the context of fluid dynamics, the maximum entropy fluid closure was first derived in Levermore (1996) as an alternative to the traditional Chapman-Enskog and Grad approaches (Chapman & Cowling, 1970; Grad, 1949b). It is a non-perturbative closure and is constructed to ensure the positivity of the distribution function f and the hyperbolicity of the convective part of the fluid equations obtained. Here we briefly review the derivation of the moment equations.

Because the closures we discuss are also applicable to neutral fluids, we start, for simplicity, with the Boltzmann equation for a single particle phase space distribution $f(\vec{x}, \vec{v}, t)$,

$$\frac{\partial f}{\partial t} + \vec{v} \cdot \nabla f = \mathcal{C}(f). \quad (1)$$

Here f is the single-particle phase space density and $\mathcal{C}(f)$ is a collision operator, assumed to conserve number, momentum, and energy. The evolution of fluid quantities is obtained by taking moments of this equation to get the hierarchy of fluid equations (Grad, 1949b; Levermore, 1996).

$$\begin{aligned} \frac{\partial n}{\partial t} + \nabla \cdot (n \vec{v}) &= 0 \\ \frac{\partial n m \vec{v}}{\partial t} + \nabla \cdot (\vec{P} + n m \vec{v} \vec{v}) &= 0 \\ &\vdots \end{aligned} \quad (2)$$

Here n is the number density, \vec{v} is the fluid velocity, and \vec{P} is the pressure tensor.

More generally, one can write

$$\frac{\partial \vec{U}}{\partial t} + \nabla \cdot \vec{F} = \vec{S}, \quad (3)$$

where \vec{U} is the vector of moments of the distribution function, \vec{F} is the vector of the associated fluxes, and \vec{S} the vector of source terms arising from moments of the collision operator. The time evolution of each fluid quantity depends on the flux term, which contains higher velocity moments. There are thus more moments than equations, and it is necessary to describe the unknown higher moments in terms of some other quantities (usually lower moments) to close the equations.

In the collisional limit, where distributions are not far from Maxwellian, the Chapman-Enskog approach can be used (Chapman & Cowling, 1970). Deviations from local equilibrium are expanded in powers of the Knudsen number ϵ , which describes the ratio of the mean free path to the gradient scale.

$$f_{CE}(\vec{x}, \vec{v}, t) = f_M(\vec{x}, \vec{v}, t)(1 + \epsilon f^{(1)} + \epsilon^2 f^{(2)} + \dots), \quad (4)$$

$$f_M(\vec{x}, \vec{v}, t) = \frac{m^{3/2} n(\vec{x}, t)}{(2\pi T(\vec{x}, t))^{3/2}} \exp\left(\frac{-m|\vec{v} - \vec{u}(\vec{x}, t)|^2}{2T(\vec{x}, t)}\right)$$

The fluid equations are closed by solving for the perturbed distribution function, leading to the Euler, Navier-Stokes, and Burnett equations at zeroth, first, and second orders, respectively. However, at second order and beyond, the equations are affected by short wavelength instabilities (Bobylev, 2008).

The Grad approach uses an expansion of the distribution function in Hermite polynomials about a local Maxwellian (Grad, 1949b) and truncating at the desired order. This is written as

$$f_{Grad}(\vec{v}) = f_M(\vec{v}) \sum_{n=0}^{\infty} \frac{1}{n!} \alpha_i^{(n)} H_i^{(n)}\left(\frac{\vec{w}}{v_t}\right), \quad (5)$$

where $\vec{w} = \vec{v} - \vec{u}(\vec{x}, t)$ and $H_i^{(n)}$ are multivariate Hermite polynomials (Grad, 1949a). The coefficients α are determined from the moments of the distribution function. The Hermite expansion has been used to investigate velocity space cascades in distribution functions (Servidio et al., 2017), but the derivation of fluid equations using Grad's model has difficulties. Away from equilibrium, there are regions of parameter space where the equations have complex characteristic velocities (Brown, 1996; Cai et al., 2015; Levermore, 1996). Additionally, the distribution functions can become negative in regions of phase space, due to the presence of odd degree polynomials in the Hermite expansion. Even so, there has been work on deriving regularized moment equations (Cai et al., 2015; Struchtrup & Torrilhon, 2003; Torrilhon & Struchtrup, 2004) and work on using non-Grad distribution functions to close the equations (Öttinger, 2010; Singh & Agrawal, 2016; Torrilhon, 2010). A particular distribution function and closure that has been used in both hydrodynamics (Torrilhon, 2010) and plasma physics (Miller & Shumlak, 2016) is the Pearson-IV distribution (Pearson, 1895), which leads to 13-moment equations (including the heat flux vector and pressure tensor). This can be written explicitly in three dimensions as

$$f_P(\vec{v}, \lambda, \vec{A}, m, \nu, \vec{n}) = \frac{1}{\det(\vec{A})} \frac{\exp\left(-\nu \arctan\left(\vec{n}^T \vec{A}^{-1}(\vec{v} - \lambda)\right)\right)}{\left(1 + (\vec{v} - \lambda)^T \vec{A}^{-2}(\vec{v} - \lambda)\right)}. \quad (6)$$

Here \vec{v} is the velocity variable, and \vec{A} is a 3×3 matrix associated with the temperature. λ and \vec{n} are vector parameters while m and ν are scalars. Compared with the Grad 13-moment equations, the equations obtained using the Pearson-IV closure have a wider region of hyperbolicity, but this requires solving for the closure parameters. As there are 14 parameters in the distribution but 13 equations, a closure must still be chosen. In this work, we use the “realizable” closure discussed in Torrilhon (2010).

In contrast to the previous approaches, the maximum entropy approach introduced by Levermore (1996) is non-perturbative and uses a distribution function

$$f(\alpha, \vec{v}) = \exp(\vec{\alpha}^T \vec{m}(\vec{v})), \quad (7)$$

where $\vec{m}(\vec{v})$ is a vector containing monomials up to a certain degree of the particle velocity components and $\vec{\alpha}$ is a vector of closure coefficients (Levermore, 1996).

For the distribution function to remain finite, as $v \rightarrow \infty$, the polynomial in the exponent must be of an even degree (Levermore, 1996). In three dimensions, the lowest-order solutions have maximum degree 2, leading to the five- and ten-moment closures, in which the density, momentum, and scalar or tensor pressures are evolved. At maximum degree 4, the 14-, 21-, 26-, and 35-moment systems are obtained (Levermore, 1996). In this work, we use the 5-, 10-, 14-, 21-, and 35-moment models. With the 14-moment model, the vector $Q_i = m \int f v^2 v_i d^3 \vec{v}$ and the scalar fourth moment $R = m \int f v^4 d^3 \vec{v}$ are used. The 21-moment model uses the scalar R as well as the tensor $Q_{ijk} = m \int f v_i v_j v_k d^3 \vec{v}$. The 35-moment model includes the heat flux tensor but uses a tensor $R_{ijkl} = m \int f v_i v_j v_k v_l d^3 \vec{v}$ instead of a scalar r . By integrating using the deviation from the mean velocities rather than \vec{v} , information about the heat flux and kurtosis, which provides information about the weight of the tails of the distribution (Westfall, 2014), are obtained.

The free parameters in this closure model are the coefficients $\vec{\alpha}$, which are calculated by maximizing the entropy given the known moments of the distribution. We briefly reproduce the derivation (Levermore, 1996) here.

Using the form of the distribution function given above, the moment equations can be rewritten as

$$\frac{\partial \langle \vec{m}(\vec{v}) f(\alpha, \vec{v}) \rangle}{\partial t} + \nabla \cdot \langle \vec{v} \vec{m}(\vec{v}) f(\alpha, \vec{v}) \rangle = \langle \vec{m}(\vec{v}) \mathcal{E}(f(\alpha, \vec{v})) \rangle, \quad (8)$$

where the angled brackets indicate integration over velocity space.

From here, we omit the \vec{v} argument and let $h(\vec{\alpha}) = \langle f(\vec{\alpha}) \rangle$ and $\vec{j}(\vec{\alpha}) = \langle \vec{v} f(\vec{\alpha}) \rangle$. These are denoted as the density and flux potentials, respectively, in Levermore (1996). Here we can see that the α derivatives of these quantities give the moment and flux terms in Equations (8). Thus, the moment equations can be written as

$$\partial_t h_\alpha + \nabla \cdot \vec{j}_\alpha = \vec{S}(\alpha). \quad (9)$$

Equation 9 can be rewritten as

$$h_{\alpha\alpha}(\vec{\alpha}) \partial_t \vec{\alpha} + \vec{j}_{\alpha\alpha}(\vec{\alpha}) \cdot \nabla \vec{\alpha} = \vec{S}(\alpha). \quad (10)$$

This ensures hyperbolicity as $h_{\alpha\alpha}(\vec{\alpha})$ is positive definite and $j_{\alpha\alpha}(\vec{\alpha})$ is symmetric.

The closure coefficients α are determined through the minimization of the quantity $h(\alpha) - \langle \alpha^T \vec{m} f(\alpha) \rangle$ with respect to α . This maximizes the entropy $-\langle f \log f - f \rangle$ given the constraint of the known moments (Levermore, 1996). The remaining quantities in the moment equations can then be calculated using this distribution.

For five and ten moments, there are closed form solutions, giving the isotropic Maxwellian $f_5(\vec{v}) = f_M(\vec{v})$ and the generalized Gaussian distribution

$$f_{10}(\vec{v}) = \frac{n}{\sqrt{(2\pi)^3 \det(\Theta)}} \exp\left(-\frac{1}{2}(\vec{v} - \vec{u})^T \Theta^{-1}(\vec{v} - \vec{u})\right), \quad (11)$$

where Θ is a positive definite matrix.

There are no closed form solutions for systems keeping moments with degree greater than 2, and it is necessary to calculate the coefficients numerically (Levermore, 1996) or make approximations to find the

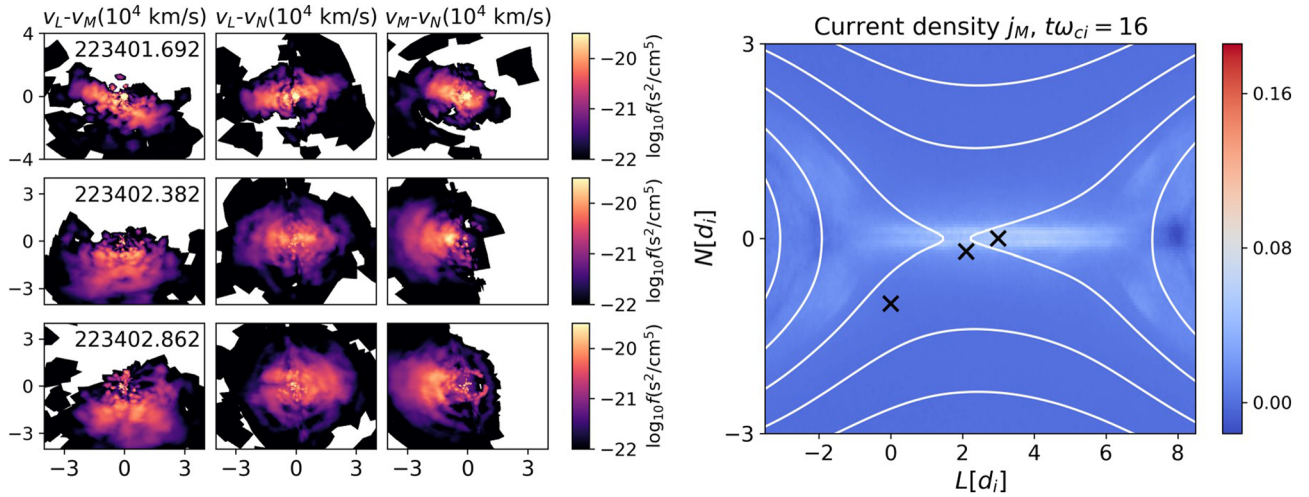


Figure 1. (Left) Electron velocity distributions measured by MMS 3 in the reconnection region at the listed times. The first row is from the inflow, the second is from approximately 12.5 km below the neutral line (Bessho et al., 2018), and the third is from the exhaust in the electron diffusion region. Each plot shows the velocity distribution integrated over the third velocity dimension. (Right) Structure of the reconnecting current sheet from the kinetic simulation. The crosses mark points where the electron distribution functions are compared.

remaining quantities to close the fluid equations (McDonald, 2016; McDonald & Torrilhon, 2013; Tensuda et al., 2016). It has also been shown that there can exist physically realizable states which cannot be described by Equation 7, though it is possible to guarantee realizability by slightly modifying the distribution (Groth & McDonald, 2009; Junk, 1998; McDonald & Groth, 2013; Schaerer & Torrilhon, 2015).

3. Reconstruction of Distributions in Reconnection Regions

During the MMS encounter with an electron diffusion region described in Torbert et al. (2018), highly non-Maxwellian electron distribution functions were observed close to the x-point. These velocity distributions have been studied in detail (Bessho et al., 2018), and it has been shown that the combination of the electron meandering motion and reconnection electric field is important for setting the structure of the distribution functions. These distributions are used to identify regions in the simulation for study and provide a link to reality.

We focus on understanding what aspects of the distribution function in this reconnection region successively higher-moment models can capture compared with kinetic simulations. To that end, we use the three distributions corresponding to the inflow, below the x-point and exhaust regions shown in Figure 1, and perform fully kinetic PIC simulations for comparison. The known moments are then used to reconstruct distributions using the maximum entropy model for various numbers of moments. Aside from the usual isotropic Maxwellian, we use the 10-, 14-, 21-, and 35-moment models, which have important properties in fluid simulations. The 10-moment model is being used in global simulations of magnetospheres (Dong et al., 2019; Wang et al., 2018) and includes the pressure tensor, which is important for balancing the reconnection electric field in collisionless reconnection. The 14- and 21-moment models include the heat flux vector and tensor, respectively, and it has been shown that capturing the heat flux correctly is important for reproducing the reconnection rate observed in kinetic simulations (Allmann-Rahn et al., 2018; Ng et al., 2017). The 35-moment model extends our previous study (Ng et al., 2018) by including the tensor $\overline{v v v v}$ moment instead of a scalar v^4 .

The simulations are performed using the PIC code PSC (Germaschewski et al., 2016). The initial condition is a Harris sheet (Harris, 1962), with $m_i/m_e = 100$, $\omega_{pe}/\omega_{ce} = 2$, and $T_i/T_e = 5$ with a background density $n_b/n_0 = 0.05$. We use the LMN coordinate system, where L is in the outflow direction, M is out-of-plane, and N is in the inflow direction, and the computational domain is $L_L \times L_N = 51.2d_i \times 12.8d_i$ resolved by $2,048 \times 512$ cells. The time step is $\Delta t = 0.17\omega_{pe}^{-1}$. Reconnection is initiated by a small magnetic field perturbation. Particles from the kinetic simulations are chosen from regions corresponding to the observed

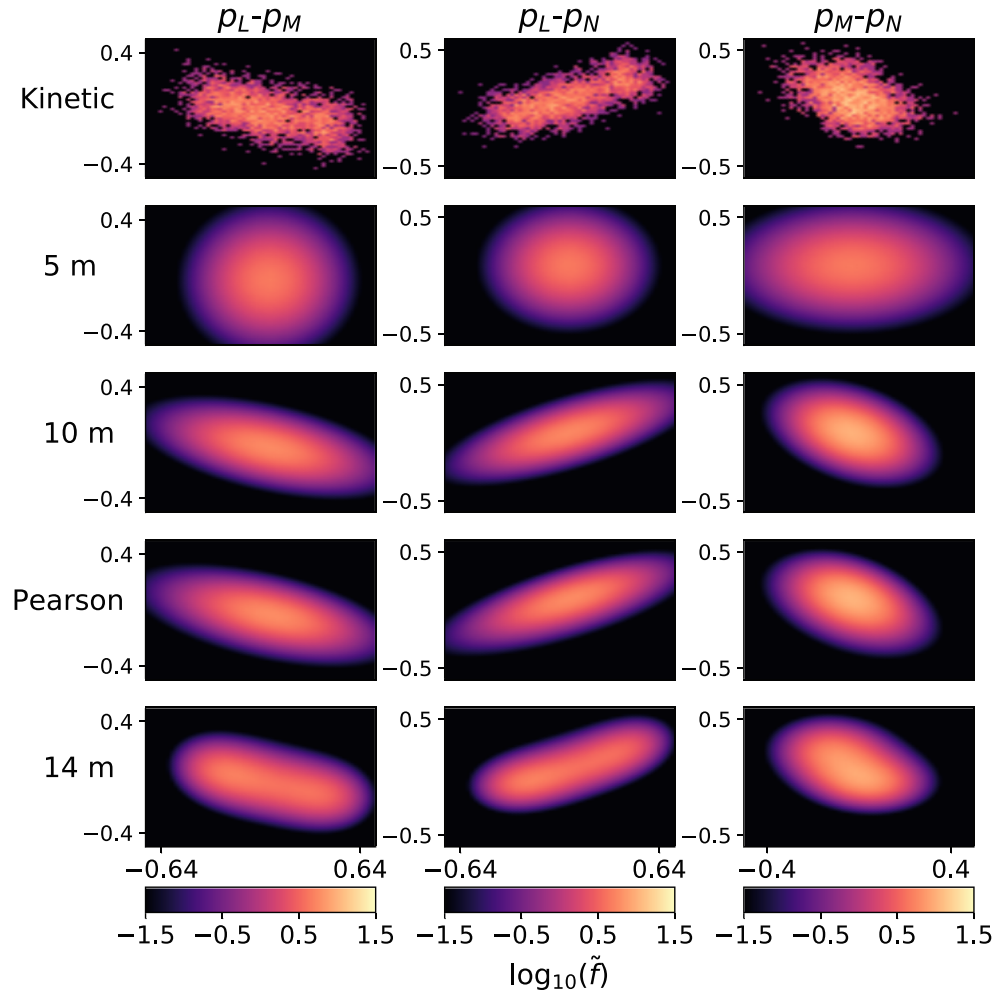


Figure 2. Comparisons of electron distributions from the kinetic simulation and reconstructions using 5-moment, 10-moment, Pearson-IV, and 14-moment models. f is normalized so that the density is 1.

distributions. We sample the particles from boxes with side $3.0d_e = 0.3d_i$ around the points marked in Figure 1 at $t\omega_{ci} = 16$. There are approximately 3,500 particles in the inflow sample and more than 5,000 particles in the x-point and exhaust samples.

To calculate the closure coefficient vector α , we maximize the quantity $-\langle f \log f - f \rangle$ using an iterative method. Because the kinetic code uses an artificially reduced speed of light, allowing some electrons to be accelerated to relativistic speeds, the distribution functions presented here are in \vec{p} -space. However, the closure calculations remain the same as the model in Equation 7 is non-relativistic, and we simply use $\vec{p} = m_e \vec{v}$, with $m_e = 1$ in our simulations. We note that this method reconstructs the distribution function from only the local moments, without the need for including any information about the electromagnetic fields.

We first study the distribution in the inflow of the reconnection region. The electron velocity distribution from the Fast Plasma Investigation (Pollock et al., 2016) is shown in the first row of Figure 1. As the electrons in this region are still magnetized, a gyrotropic distribution is observed, with $P_{\parallel} > P_{\perp}$. This anisotropy is due to a combination of electrostatic and magnetic trapping (Egedal et al., 2013; Le et al., 2009).

Figure 2 shows the electron distributions obtained from the inflow of the kinetic simulation and reconstructions using the 5-, 10-, and 14-moment and Pearson-IV models. The kinetic simulation reproduces the observed anisotropy as it retains all the kinetic physics associated with the particle trapping. In reconstructing the distributions, we find that the 10-moment and Pearson-IV models are able to reproduce the anisotropy, but the v^4 moment is required to reproduce the flattening associated with the particle trapping.

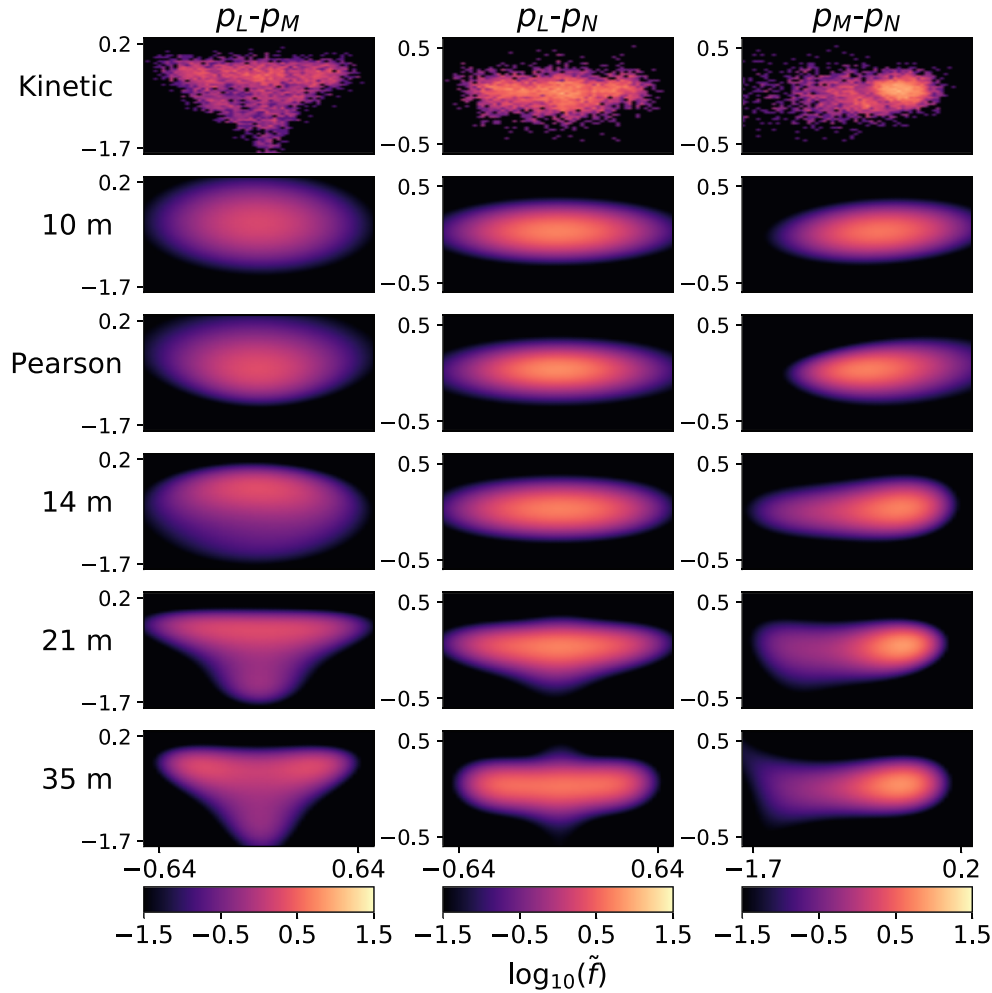


Figure 3. Comparisons of reduced electron distributions just below the x-point from the kinetic simulation and reconstructions using Pearson-IV and 10-, 14-, 21-, and 35-moment models. f is normalized so that the density is 1.

The second distribution studied is from close to the x-point. In the second row of Figure 1, which shows the electron velocity distribution from the MMS data, we observe the acceleration in the $-v_M$ direction associated with the reconnection electric field and meandering motion, the spread in v_L compared with v_N due to the upstream pressure anisotropy, and the multiple populations in the v_M – v_N plane associated with the number of times electrons have meandered (Bessho et al., 2014, 2018; Fujimoto & Sydora, 2009; Ng et al., 2011, 2012). The slight asymmetry in v_N and lack of counterstreaming populations show that the distribution is taken from below the x-point.

In Figure 3, we show the structure of the particle distribution from the kinetic simulation and the reconstructions using the moment models. Similarly to (Ng et al., 2018), the reproduction of the triangular shape associated with the acceleration requires the full heat flux tensor (using the 21- or 35-moment model). Although the 14-moment model is unable to reproduce the triangular shape, the accelerated population of electrons is still present as seen in the rightmost column, and while the Pearson-IV distribution does show some asymmetry in the p_M direction, it is not distorted to the extent of the 14-moment distribution nor does it show the acceleration in the negative M direction. The inclusion of the tensor v^4 moment compared with the scalar v^4 does not make a big difference to the reconstruction for this region. In all cases, the structures associated with multiple electron crossings of the current sheet seen in the kinetic results are not reproduced.

The final comparison of the electron distributions is between distributions in the exhaust approximately $7d_e$ downstream of the x-point. The bottom row of Figure 1 shows the velocity distribution taken from MMS, where the distribution has been accelerated in the L direction due to the turning of v_M into v_L by B_N .

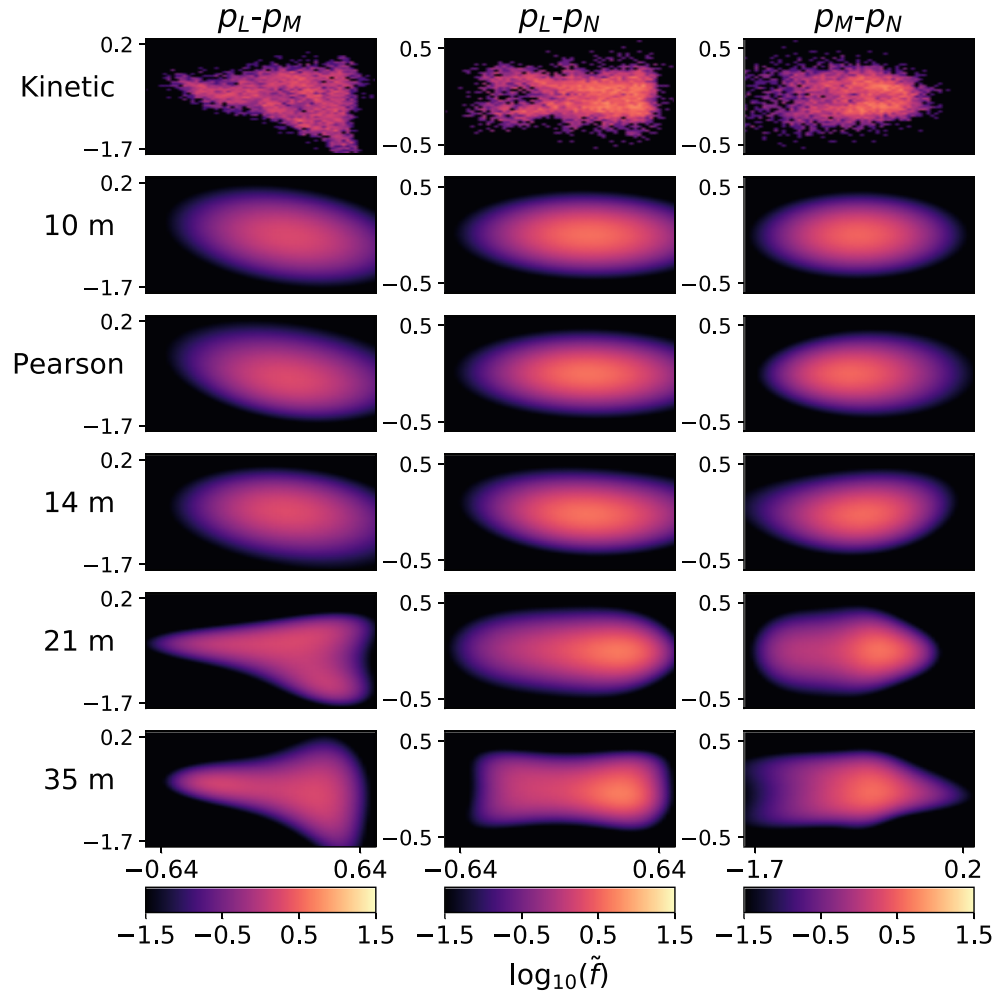


Figure 4. Comparisons of reduced electron distributions in the exhaust from the kinetic simulation and reconstructions using Pearson-IV and 10-, 14-, 21-, and 35-moment models. f is normalized so that the density is 1.

There are counterstreaming populations in the N direction due to the meandering of the electrons, indicating that this point is closer to the neutral line. These are most visible in the v_L - v_N plot.

The results of the kinetic simulation and moment reconstructions are shown in Figure 4. In the kinetic simulation, the triangular shape is maintained and rotated in the positive v_L direction (Bessho et al., 2014; Ng et al., 2011). Once again, the 10- and 14-moment and Pearson-IV models do not capture the triangular shape of the distribution, while the 21- and 35-moment models manage to do so. The counterstreaming populations seen in the LN distribution are not reproduced even using the 35-moment model, though the separation of the distribution into two peaks can be seen in cuts at larger p_L and broadening of the distribution in the N direction compared with the 21-moment model is observed. This is because the inclusion of the fourth-order tensor provides additional information about the tails of the distribution in the different directions rather than just isotropically. It is likely that the counterstreaming populations would be captured if the separation of the populations were greater, as it has been shown that in one dimension, counterstreaming populations in hydrodynamic simulations can be captured by 14-moment simulations (Forgues & McDonald, 2019). We illustrate this using a reconstruction of the ion distribution at the x-point.

Figure 5 shows the reduced distributions of ions taken from the x-point. Since ions and electrons have opposite charge, the acceleration by the reconnection electric field and thus the tip of the triangular population are in the positive p_M direction. In the particle distribution, there is much clearer separation between the ions in p_N than in the electron distribution because of the lower thermal velocity of the inflowing ions

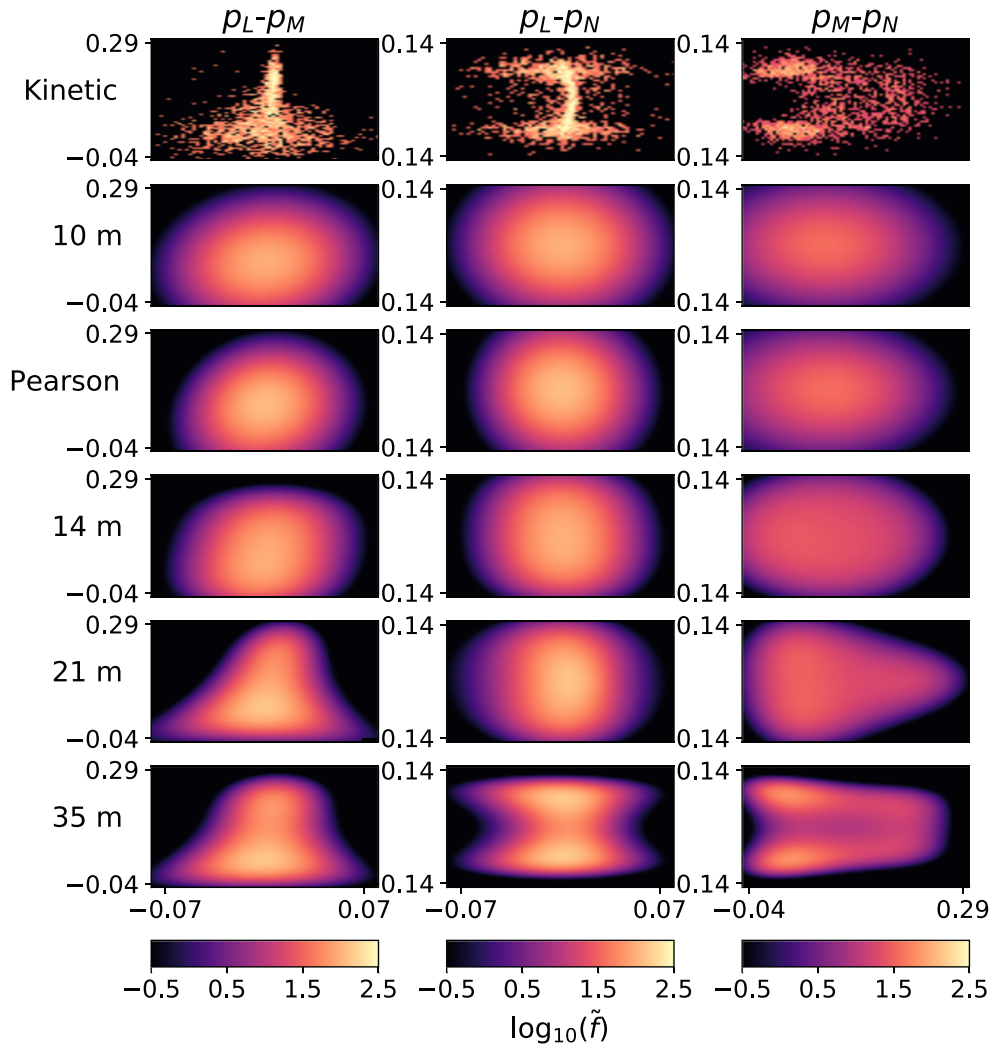


Figure 5. Comparisons of reduced ion distributions at the x-point from the kinetic simulation and reconstructions using Pearson-IV and 10-, 14-, 21-, and 35-moment models. f is normalized so that the density is 1.

compared with the bulk velocity of each counterstreaming population. This can be seen in the third column at low p_M . The results of using the 10-, 14-, and 21-moment and Pearson-IV models are similar to what is observed with the electrons, with the acceleration in p_M reproduced to varying degrees of success. In particular, there is a large spread in p_N , which would misleadingly indicate a high T_{NN} when the distribution is in fact composed of two separated colder populations. The 35-moment reconstruction shows the best agreement with the kinetic distribution and a qualitative improvement on the 21-moment model. This is clearest in the p_M-p_N plot, in which the two counterstreaming populations are visible at low p_N and the overall shape of the distribution with the broader region at large p_N is captured.

4. Conclusion

We have used successively higher numbers of moments to reconstruct electron velocity distributions in reconnection regions. The maximum entropy method, which we use, has the properties of guaranteeing the positivity of the resulting distribution and the hyperbolicity of the fluid equations obtained, but is more difficult to evaluate as no closed form solutions exist for >10 moments. This closure reconstructs the distribution from only the locally known moments without information about the electromagnetic fields or physical processes, allowing it to be used for different plasma parameters.

The use of the 35-moment model for reconstruction shows improvements over the lower-moment models for the more non-Maxwellian distributions close to the x-point and in the exhaust. This is most evident in the p_L – p_N plane, where a broadening of the distribution is observed, though the counterstreaming beams are still not reproduced. The model is also insufficient to reproduce the finer structures observed which are caused by meandering electron orbits. When modeling the ion distribution, at the x-point, the separation between the counterstreaming ion populations is larger (compared with the thermal spread of the populations), and the 35-moment model is able to capture this feature of the distribution function.

The results give insight into what physics extended fluid models, which are being developed for global simulations (Dong et al., 2019; Wang et al., 2018), are able to describe and how many variables will need to be evolved if the maximum entropy method is used. Here we see that the full fourth-order tensor is required to reproduce counterstreaming populations (which occur in reconnection regions and at shocks, for example), but this is dependent on how distinct the populations are as seen from the different results when comparing electrons and ions. We should note that the reconstruction here is a best-case scenario where the kinetic distribution is known, and it is not guaranteed that a fluid simulation would evolve to the same state self-consistently.

While this work is focused on the features of particle distributions that can be reproduced by the various models, we briefly comment on the challenges of implementation. The Pearson-IV model has been used in plasma physics to simulate some test problems (Miller & Shumlak, 2016) but still requires study for physics relevant to the magnetosphere. For the maximum entropy model, each time step would involve solving an optimization problem for the closure parameters, which is challenging and computationally intensive as shown by existing work on 35-moment models (Schaefer & Torrilhon, 2017). A possible approach is that of McDonald and Torrilhon (2013), who use a closed-form approximation of the 14-moment closure.

Data Availability Statement

Subsets of the data are available at The Digital Repository at the University of Maryland <http://hdl.handle.net/1903/25486>.

Acknowledgments

This work was supported by DOE Contract DE-AC02-09CH11466 and NSF grant AGS-1338944, DOE grant DESC0016278, NSF grant AGS-1619584, NASA grant 80NSSC18K1369. This research used resources of the National Energy Research Scientific Computing Center (NERSC), a US Department of Energy Office of Science User Facility operated under Contract No. DE-AC02-05CH11231.

References

- Allmann-Rahn, F., Trost, T., & Grauer, R. (2018). Temperature gradient driven heat flux closure in fluid simulations of collisionless reconnection. *Journal of Plasma Physics*, 84(3), 905840307. <https://doi.org/10.1017/S002237781800048X>
- Bessho, N., Chen, L.-J., Shuster, J. R., & Wang, S. (2014). Electron distribution functions in the electron diffusion region of magnetic reconnection: Physics behind the fine structures. *Geophysical Research Letters*, 41, 8688–8695. <https://doi.org/10.1002/2014GL02034>
- Bessho, N., Chen, L.-J., Wang, S., & Hesse, M. (2018). Effect of the reconnection electric field on electron distribution functions in the diffusion region of magnetotail reconnection. *Geophysical Research Letters*, 45, 12,142–12,152. <https://doi.org/10.1029/2018GL081216>
- Bobylev, A. V. (2008). Generalized burnett hydrodynamics. *Journal of Statistical Physics*, 132(3), 569–580. <https://doi.org/10.1007/s10955-008-9556-5>
- Brown, S. L. (1996). Approximate riemann solvers for moment models of dilute gases (Ph.D. Thesis).
- Cai, Z., Fan, Y., & Li, R. (2015). A framework on moment model reduction for kinetic equation. *SIAM Journal on Applied Mathematics*, 75(5), 2001–2023. <https://doi.org/10.1137/14100110X>
- Chapman, S., & Cowling, T. G. (1970). *The mathematical theory of non-uniform gases: An account of the kinetic theory of viscosity, thermal conduction and diffusion in gases*. Cambridge, England: Cambridge University Press.
- Charniak, E. (2000). A maximum-entropy-inspired parser. In *Proceedings of the 1st north american chapter of the association for computational linguistics conference* (pp. 132–139). *NAACL 2000*. Stroudsburg, PA, USA: Association for Computational Linguistics. Retrieved from <http://dl.acm.org/citation.cfm?id=974305.974323>
- Dong, C., Wang, L., Hakim, A., Bhattacharjee, A., Slavin, J. A., DiBraccio, G. A., & Germaschewski, K. (2019). Global ten-moment multifluid simulations of the solar wind interaction with mercury: From the planetary conducting core to the dynamic magnetosphere. *Geophysical Research Letters*, 46, 11,584–11,596. <https://doi.org/10.1029/2019GL083180>
- Egedal, J., Le, A., & Daughton, W. (2013). A review of pressure anisotropy caused by electron trapping in collisionless plasma, and its implications for magnetic reconnection. *Physics of Plasmas*, 20(6), 061201. <https://doi.org/10.1063/1.4811092>
- Forgues, F., & McDonald, J. G. (2019). Higher-order moment models for laminar multiphase flows with accurate particle-stream crossing. *International Journal of Multiphase Flow*, 114, 28–38. <https://doi.org/10.1016/j.ijmultiphaseflow.2019.01.003>
- Fujimoto, K. (2018). Multi-scale kinetic simulation of magnetic reconnection with dynamically adaptive meshes. *Frontiers in Physics*, 6, 119. <https://doi.org/10.3389/fphy.2018.00119>
- Fujimoto, K., & Sydora, R. D. (2009). Particle description of the electron diffusion region in collisionless magnetic reconnection. *Physics of Plasmas*, 16(11), 112309. <https://doi.org/10.1063/1.3263694>
- Germaschewski, K., Fox, W., Abbott, S., Ahmadi, N., Maynard, K., Wang, L., et al. (2016). The plasma simulation code: A modern particle-in-cell code with patch-based load-balancing. *Journal of Computational Physics*, 318, 305–326. <https://doi.org/10.1016/j.jcp.2016.05.013>
- Grad, H. (1949a). Note on n-dimensional hermite polynomials. *Communications on Pure and Applied Mathematics*, 2(4), 325–330. <https://doi.org/10.1002/cpa.3160020402>
- Grad, H. (1949b). On the kinetic theory of rarefied gases. *Communications on Pure and Applied Mathematics*, 2(4), 331–407. <https://doi.org/10.1002/cpa.3160020403>

- Groth, C. P. T., & McDonald, J. G. (2009). Towards physically realizable and hyperbolic moment closures for kinetic theory. *Continuum Mechanics and Thermodynamics*, 21(6), 467. <https://doi.org/10.1007/s00161-009-0125-1>
- Harris, E. (1962). On a plasma sheath separating regions of oppositely directed magnetic field. *Il Nuovo Cimento (1955-1965)*, 23, 115–121. <https://doi.org/10.1007/BF02733547>
- Hesse, M., Winske, D., & Kuznetsova, M. M. (1995). Hybrid modeling of collisionless reconnection in two-dimensional current sheets: Simulations. *Journal of Geophysical Research*, 100(A11), 21,815–21,825. <https://doi.org/10.1029/95JA01559>
- Ho, A., Datta, I. A. M., & Shumlak, U. (2018). Physics-based-adaptive plasma model for high-fidelity numerical simulations. *Frontiers in Physics*, 6, 105. <https://doi.org/10.3389/fphy.2018.00105>
- Jaynes, E. T. (1957). Information theory and statistical mechanics. *Physical Review*, 106, 620–630. <https://doi.org/10.1103/PhysRev.106.620>
- Junk, M. (1998). Domain of definition of Levermore's five-moment system. *Journal of Statistical Physics*, 93, 1143–1167. <https://doi.org/10.1023/B:JOSS.0000033155.07331.d9>
- Karimabadi, H., Vu, H. X., Krauss-Varban, D., & Omelchenko, Y. (2006). Global hybrid simulations of the Earth's magnetosphere. In G. P. Zank & N. V. Pogorelov (Eds.), *Numerical modeling of space plasma flows, Astronom-2006 ASP Conference Series* (Vol. 359, pp. 171). San Francisco: Astronomical Society of the Pacific.
- Kempf, Y., Pokhotelov, D., von Alfthan, S., Vaivads, A., Palmroth, M., & Koskinen, H. E. J. (2013). Wave dispersion in the hybrid-vlasov model: Verification of vlasior. *Physics of Plasmas*, 20(11), 112114. <https://doi.org/10.1063/1.4835315>
- Lautenbach, S., & Grauer, R. (2018). Multiphysics simulations of collisionless plasmas. *Frontiers in Physics*, 6, 113. <https://doi.org/10.3389/fphy.2018.00113>
- Le, A., Egedal, J., Daughton, W., Fox, W., & Katz, N. (2009). Equations of state for collisionless guide-field reconnection. *Physical Review Letters*, 102(8), 085001. <https://doi.org/10.1103/PhysRevLett.102.085001>
- Levermore, C. D. (1996). Moment closure hierarchies for kinetic theories. *Journal of Statistical Physics*, 83(5), 1021–1065. <https://doi.org/10.1007/BF02179552>
- Lu, S., Lin, Y., Lu, Q. M., Wang, X. Y., Wang, R. S., Huang, C., et al. (2015). Evolution of flux ropes in the magnetotail: A three-dimensional global hybrid simulation. *Physics of Plasmas*, 22(5), 052901. <https://doi.org/10.1063/1.4919615>
- McDonald, J. G. (2016). Approximate maximum-entropy moment closures for gas dynamics. *AIP Conference Proceedings*, 1786(1), 140001. <https://doi.org/10.1063/1.4967632>
- McDonald, J. G., & Groth, C. P. T. (2013). Towards realizable hyperbolic moment closures for viscous heat-conducting gas flows based on a maximum-entropy distribution. *Continuum Mechanics and Thermodynamics*, 25(5), 573–603. <https://doi.org/10.1007/s00161-012-0252-y>
- McDonald, J., & Torrilhon, M. (2013). Affordable robust moment closures for cfd based on the maximum-entropy hierarchy. *Journal of Computational Physics*, 251, 500–523. <https://doi.org/10.1016/j.jcp.2013.05.046>
- Miller, S. T., & Shumlak, U. (2016). A multi-species 13-moment model for moderately collisional plasmas. *Physics of Plasmas*, 23(8), 82,303. <https://doi.org/10.1063/1.4960041>
- Ng, J., Egedal, J., Le, A., & Daughton, W. (2012). Phase space structure of the electron diffusion region in reconnection with weak guide fields. *Physics of Plasmas* (1994-present), 19(11), 112108. <https://doi.org/10.1063/1.4766895>
- Ng, J., Egedal, J., Le, A., Daughton, W., & Chen, L.-J. (2011). Kinetic structure of the electron diffusion region in antiparallel magnetic reconnection. *Physical Review Letter*, 106, 065002. <https://doi.org/10.1103/PhysRevLett.106.065002>
- Ng, J., Hakim, A., & Bhattacharjee, A. (2018). Using the maximum entropy distribution to describe electrons in reconnecting current sheets. *Physics of Plasmas*, 25(8), 082113. <https://doi.org/10.1063/1.5041758>
- Ng, J., Hakim, A., Bhattacharjee, A., Stanier, A., & Daughton, W. (2017). Simulations of anti-parallel reconnection using a nonlocal heat flux closure. *Physics of Plasmas*, 24(8), 082112. <https://doi.org/10.1063/1.4993195>
- Ng, J., Hakim, A., Juno, J., & Bhattacharjee, A. (2019). Drift instabilities in thin current sheets using a two-fluid model with pressure tensor effects. *Journal of Geophysical Research: Space Physics*, 124, 3331–3346. <https://doi.org/10.1029/2018JA026313>
- Øieroset, M., Lin, R. P., Phan, T. D., Larson, D. E., & Bale, S. D. (2002). Evidence for electron acceleration up to ~ 300 KeV in the magnetic reconnection diffusion region of earth's magnetotail. *Physical Review Letters*, 89, 195001. <https://doi.org/10.1103/PhysRevLett.89.195001>
- Öttinger, H. C. (2010). Thermodynamically admissible 13 moment equations from the boltzmann equation. *Physical Review Letters*, 104, 120601. <https://doi.org/10.1103/PhysRevLett.104.120601>
- Palmroth, M., Ganse, U., Pfau-Kempf, Y., Battarbee, M., Turc, L., Brito, T., et al. (2018). Vlasov methods in space physics and astrophysics. *Living reviews in computational astrophysics*, 4(1), 1. <https://doi.org/10.1007/s41115-018-0003-2>
- Pearson, K. (1895). X. contributions to the mathematical theory of evolution.ii. skew variation in homogeneous material. *Philosophical Transactions of the Royal Society of London (A)*, 186, 343–414.
- Pollock, C., Moore, T., Jacques, A., Burch, J., Gliese, U., Saito, Y., et al. (2016). Fast plasma investigation for magnetospheric multiscale. *Space Science Reviews*, 199(1-4), 331–406.
- Richstone, D. O., & Tremaine, S. (1988). Maximum-entropy models of galaxies. *The Astrophysical Journal*, 327, 82–88. <https://doi.org/10.1086/166171>
- Schaerer, R. P., & Torrilhon, M. (2015). On singular closures for the 5-moment system in kinetic gas theory. *Communications in Computational Physics*, 17(2), 371400. <https://doi.org/10.4208/cicp.201213.130814>
- Schaerer, R. P., & Torrilhon, M. (2017). The 35-moment system with the maximum-entropy closure for rarefied gas flows. *European Journal of Mechanics - B/Fluids*, 64, 30–40. <https://doi.org/10.1016/j.euromechflu.2017.01.003>
- Servidio, S., Chasapis, A., Matthaeus, W. H., Perrone, D., Valentini, F., Parashar, T. N., et al. (2017). Magnetospheric multiscale observation of plasma velocity-space cascade: Hermite representation and theory. *Physical Review Letters*, 119, 205101. <https://doi.org/10.1103/PhysRevLett.119.205101>
- Singh, N., & Agrawal, A. (2016). Onsager's-principle-consistent 13-moment transport equations. *Physical Review E*, 93, 063111. <https://doi.org/10.1103/PhysRevE.93.063111>
- Struchtrup, H., & Torrilhon, M. (2003). Regularization of grad's 13 moment equations: Derivation and linear analysis. *Physics of Fluids*, 15(9), 2668–2680. <https://doi.org/10.1063/1.1597472>
- Tensuda, B. R., McDonald, J. G., & Groth, C. P. T. (2016). Multi-dimensional validation of a maximum-entropy-based interpolative moment closure. *AIP Conference Proceedings*, 1786(1), 140008. <https://doi.org/10.1063/1.4967639>
- Torbert, R. B., Burch, J. L., Phan, T. D., Hesse, M., Argall, M. R., Shuster, J., et al. (2018). Electron-scale dynamics of the diffusion region during symmetric magnetic reconnection in space. *Science*, 362(6421), 1391–1395. <https://doi.org/10.1126/science.aat2998>
- Torrilhon, M. (2010). Hyperbolic moment equations in kinetic gas theory based on multi-variate pearson-iv-distributions. *Communications in Computational Physics*, 7(4), 639–673.

- Torrilhon, M., & Struchtrup, H. (2004). Regularized 13-moment equations: Shock structure calculations and comparison to burnett models. *Journal of Fluid Mechanics*, 513, 171–198. <https://doi.org/10.1017/S0022112004009917>
- Tóth, G., Chen, Y., Gombosi, T. I., Cassak, P., Markidis, S., & Peng, I. B. (2017). Scaling the ion inertial length and its implications for modeling reconnection in global simulations. *Journal of Geophysical Research: Space Physics*, 122, 10,336–10,355. <https://doi.org/10.1002/2017JA024189>
- Tóth, G., Jia, X., Markidis, S., Peng, I. B., Chen, Y., Daldorff, L. K. S., et al. (2016). Extended magnetohydrodynamics with embedded particle-in-cell simulation of ganymede's magnetosphere. *Journal of Geophysical Research: Space Physics*, 121, 1273–1293. <https://doi.org/10.1002/2015JA021997>
- Wang, L., Germaschewski, K., Hakim, A., Dong, C., Raeder, J., & Bhattacharjee, A. (2018). Electron physics in 3-d two-fluid 10-moment modeling of ganymede's magnetosphere. *Journal of Geophysical Research: Space Physics*, 123, 2815–2830. <https://doi.org/10.1002/2017JA024761>
- Wang, L., Hakim, A. H., Bhattacharjee, A., & Germaschewski, K. (2015). Comparison of multi-fluid moment models with particle-in-cell simulations of collisionless magnetic reconnection. *Physics of Plasmas (1994-present)*, 22(1), 012108. <https://doi.org/10.1063/1.4906063>
- Westfall, P. H. (2014). Kurtosis as peakedness, 1905–2014. r.i.p. *The American Statistician*, 68(3), 191–195. <https://doi.org/10.1080/00031305.2014.917055>
- Yeo, G., & Burge, C. B. (2004). Maximum entropy modeling of short sequence motifs with applications to rna splicing signals. *Journal of Computational Biology*, 11(2-3), 377–394. <https://doi.org/10.1089/1066527041410418>
- Yin, L., Winske, D., Gary, S. P., & Birn, J. (2001). Hybrid and hall-mhd simulations of collisionless reconnection: Dynamics of the electron pressure tensor. *Journal of Geophysical Research*, 106(A6), 10,761–10,775. <https://doi.org/10.1029/2000JA000398>